Implementation of a Neural Network for Multispectral Luminescence Imaging of Lake Pigment Paints

Camille Simon Chane,[a,*] Mathieu Thoury,[b,†] Aurélie Tournié,[b] Jean-Philippe Echard[a]

[a] *Musée de la musique, Equipe Conservation Recherche, Cité de la musique, 221 avenue Jean Jaurès, 75019 Paris, France*
[b] *Centre de Recherche sur la Conservation des Collections MNHN / CNRS / MCC, 36 rue Geoffroy Saint-Hilaire, 75005 Paris, France*

Luminescence multispectral imaging is a developing and promising technique in the fields of conservation science and cultural heritage studies. In this article, we present a new methodology for recording the spatially resolved luminescence properties of objects. This methodology relies on the development of a lab-made multispectral camera setup optimized to collect low-yield luminescence images. In addition to a classic data preprocessing procedure to reduce noise on the data, we present an innovative method, based on a neural network algorithm, that allows us to obtain radiometrically calibrated luminescence spectra with increased spectral resolution from the low-spectral resolution acquisitions. After preliminary corrections, a neural network is trained using the 15-band multispectral luminescence acquisitions and corresponding spot spectroscopy luminescence data. This neural network is then used to retrieve a megapixel multispectral cube between 460 and 710 nm with a 5 nm resolution from a low-spectral-resolution multispectral acquisition. The resulting data are independent from the detection chain of the imaging system (filter transmittance, spectral sensitivity of the lens and optics, etc.). As a result, the image cube provides radiometrically calibrated emission spectra with increased spectral resolution. For each pixel, we can thus retrieve a spectrum comparable to those obtained with conventional luminescence spectroscopy. We apply this method to a panel of lake pigment paints and discuss the pertinence and perspectives of this new approach.

Index Headings: **Multispectral imaging; Luminescence imaging; Pigment; Binder; In situ analysis; Cultural heritage.**

INTRODUCTION

The luminescence properties of painting materials (pigments and binding media) have long been used to reveal or enhance the chemical contrast in polychrome objects and easel paintings.[1] The visual observation of ultraviolet (UV)-induced luminescence and the capture of UV-induced color photography are now routine practices in conservation studios to evidence restoration materials and to localize luminescent pigments and binding media on paintings. These techniques are also used in violin-making workshops to assess the extent of interventions on the varnish of centuries-old instruments.[2,3] However, a color visually perceived under UV illumination cannot be unequivocally associated with a material or a class of materials, even though it is tempting to make such correlations.

Developments in luminescence spectroscopy have provided access to quantitative data that can be used for the characterization of pigments and organic media encountered on heritage artifacts.[4–8] The luminescence features of some artists' and artisan materials are diverse, relatively sharp with a full width at half-maximum (FWHM) that can be less than 40 nm, or complex,[6,9] whereas those of the binding media are generally broad[7] (FWHM of 70 nm or more).

In situ fiber optic spectrofluorometers have been developed to perform analyses directly on works of art.[10,11] Implemented in microscope setups, spectrofluorimeters allow the acquisition of luminescence features of micrometer-scale areas on cross-section samples of painting.[12,13] However, there are several drawbacks inherent to spot analysis. The choice of the analysis positions (typically a few tens per work of art) depends on the prior estimation by the operator of the diversity of the expected spectra. When spot analysis follows an imaging acquisition, we expect the analysis positions to be representative of the larger area identified by the imaging, which generally has limited spectral resolution. It may also be difficult to accurately localize spot-acquisition positions. Spot acquisitions are thus time consuming. Most important, by definition only a limited area is analyzed. To our knowledge, there has been no report of the raster-scanning of a surface using a fiber optics probe (at the macro-scale) in the study of cultural artifact surfaces.

Alternative strategies have been developed to overcome the limitations intrinsic to spot analysis and to embrace the spatial heterogeneity of cultural heritage objects.[14] The most widespread approach has been to use multispectral luminescence imaging systems to study model paints[15] as well as wall and easel paintings.[8,16–19] A fluorescence-lifetime imaging system has also been developed to image the distribution of luminophores over an area of a few tens of square centimeters according to their luminescence decay.[20] Such approaches can be implemented from the macro- down to the micro-scale using microscope setups, for instance to study minute cross-section samples to reveal a paint stratigraphy.[21] Recent developments have included an interest in coupling a synchrotron beam with optimized microspectroscopy and micro-imaging setups to study the luminescence of organic and inorganic materials on the submicro-scale.[9,22]

There is a great diversity both in the use made of multispectral data and in their possible processing, independent of the artifacts studied and the analytical approaches used. The first step in multispectral data processing is usually a noise reduction of the images collected. A second step may be necessary, depending on

Received 31 March 2014; accepted 28 September 2014.
* Author to whom correspondence should be sent. E-mail: csimonchane@cite-musique.fr.
† Current address: IPANEMA USR 3461 CNRS / MCC, BP48 Saint-Aubin, 91192 Gif-sur-Yvette, France.
DOI: 10.1366/14-07554

0003-7028/15/6904-0430/0

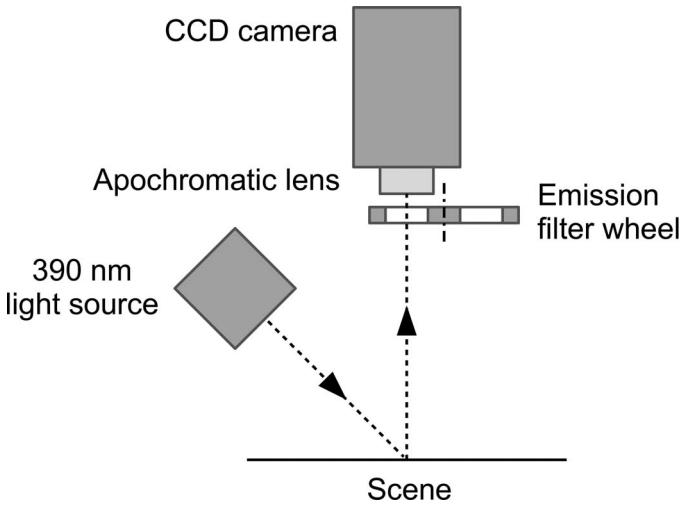

FIG. 1. Multispectral acquisition setup.

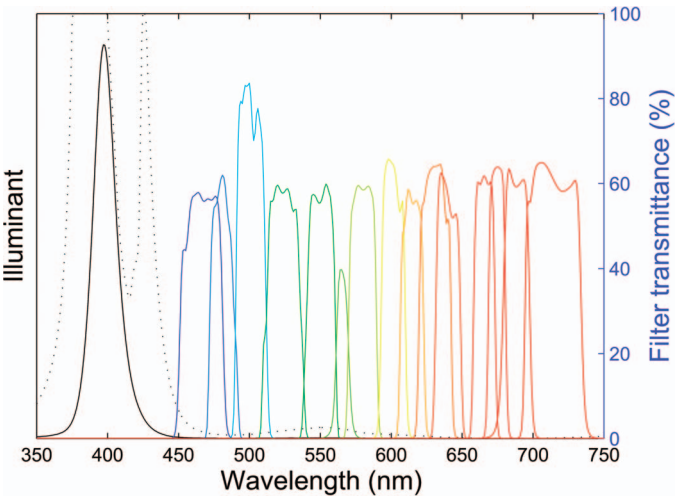

FIG. 2. Emission spectrum of the LED used in the multispectral setup (black). The dashed line represents a zoom 25 times in intensity and highlights the secondary emission peak. The transmittance of the bandpass filters used for the multispectral camera are plotted from blue to red.

the acquisition paradigm; in the case of band per band imaging, it is mandatory to perform a spatial registration of the images collected. This step is not necessary in the case of raster-scanning multispectral acquisitions. We grouped these two steps, which are the same as those generally performed in reflection multispectral imaging, under the term "preliminary corrections". Because luminescence intensity yields are, in general, two orders of magnitude lower than reflection yields, it is crucial that these corrections be carefully performed. Surprisingly, these preliminary corrections are rarely detailed in the literature; it is thus difficult to evaluate their relevance.

In addition to the preliminary corrections necessary to reduce the noise in the data, there are two nonexclusive approaches generally employed for the apprehension of multispectral data, and in particular multispectral luminescence data. The first is to classify the preprocessed data using data-mining techniques, such as those performed by Delaney et al.[19] The second approach consists in correcting the preprocessed data to obtain quantitative data that are comparable to the intrinsic luminescence features of the materials, as obtained using luminescence spectroscopy; this was performed by Bertrand et al.[9] In addition, recent approaches have focused on the development of hyperspectral imaging systems that directly provide data with high spatial and spectral resolution, although this remains a technological challenge.[23,24] Luminescence hyperspectral imaging has been rarely tackled because the narrowness of FWHM of hyperspectral band makes it very difficult to detect signals from solid-state materials with low quantum yields.[15]

Our approach consists of combining luminescence spot spectroscopy and multispectral imaging to obtain luminescence spectroscopic data with high spectral resolution and megapixel information describing a surface. The use of spot spectroscopy to enhance multispectral data has been investigated with interesting results in the case of reflection measurements.[25–27]

We first present the acquisition systems used—a multispectral camera with a reduced number of bands (15) and a spot spectrometer. Then we describe the preprocessing of the multispectral acquisitions. We detail and justify the use of a neural network adapted to the specificities of luminescence characterization. The methodology is then evaluated on a sample panel painted using lake-containing paints typically encountered in 15th- to 19th-century European easel paintings.[28] Some patches of the panel were used to provide training data for the neural network, while the others were used to evaluate the quality of the reconstruction.

EXPERIMENTAL

Two acquisition systems were employed: a lab-designed multispectral acquisition system that collected full-field images of the scene in 15 spectral bands covering the 450–740 nm range and a fiber optic spectrometer that collected luminescence spectra.

Multispectral Imaging. The full-field multispectral acquisition system consisted of a camera, a camera lens, a filter wheel, and bandpass interference filters. It was designed following principles similar to other lab-designed systems.[17,29–31] The 1.4 Mpixel 12-bit charge-coupled device (CCD) camera (Retiga SRV, QImaging) has an increased quantum efficiency in the 500–1000 nm range, making it well adapted to low light and luminescence imaging. This detector was used in conjunction with a 23 mm apochromatic lens (APO-XenoPlan, Schneider-Kreuznach), selected to minimize chromatic and spherical aberrations. Finally, a manual filter wheel, placed in front of the lens, allowed the sequential positioning of a series of interference bandpass filters (Omega) in the optical path. This multispectral setup is shown Fig. 1. An acquisition consisted of a series of grayscale images, each in the range of a different filter. The bandpass filters were selected to cover the 450–740 nm spectral range with optimized transmittances and passbands (Fig. 2). The acquisition times per band were selected to best exploit the dynamic range of the sensor in every spectral band. The acquisition time of the images collected varied from 11 s for the filter with a

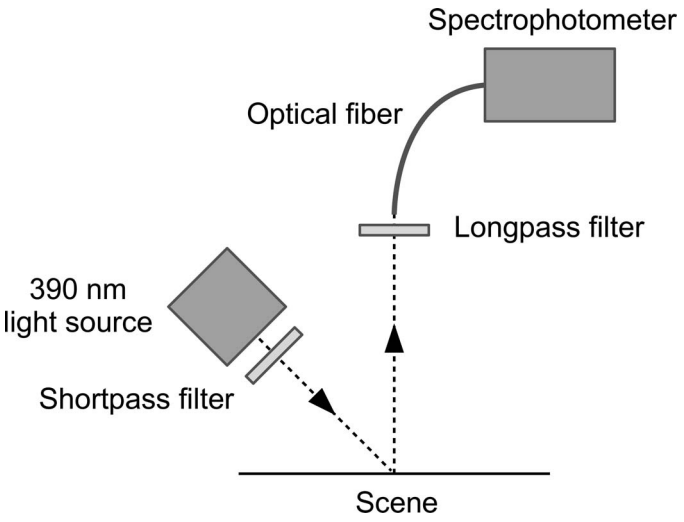

FIG. 3. Setup of acquisitions performed using a spectrometer.

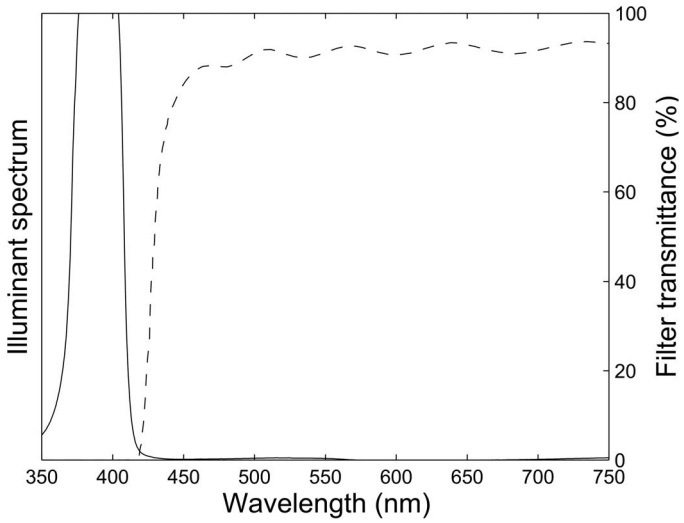

FIG. 4. Emission spectrum of the 390 nm light bulb used for the illumination filtered by the shortpass filter (solid line). The transmittance of the longpass filter is plotted with a dashed line.

central passband of 525 nm to 55 s for the filter with a central passband of 565 nm.

During this study, the object–camera distance was approximately 62 cm, resulting in a projected pixel smaller than 0.2 mm. The scene was illuminated using a 390 nm light-emitting diode (LED) source (VioLED). In addition to its main 390 nm emission, this source has a secondary emission peak around 425 nm. This secondary peak is 23 times less intense than the main peak. The illuminant also presents a weak broad contribution in the 500 nm region (Fig. 2). The light emitted by the source in the spectral range of multispectral acquisition and reflected by the object under study could contaminate luminescence multispectral acquisition. To evaluate contribution of the stray reflection to the luminescence, a 99% diffuse reflection standard (Spectralon SRS-99, Labsphere) was placed in the scene.

Fiber Optic Luminescence Spectrometry. Luminescence spectra were obtained using a fiber optic spectrometer portable fiber spectroradiometer, FieldSpec 4 (Hi-Resolution; ASD Inc.), covering the visible and near-infrared wavelengths (350–2500 nm) with a spectral resolution of 3 nm between 350 and 1000 nm (and 10 nm between 1000 and 2500 nm). This spectrometer collects light emitted from a spot of a few square millimeters and is usually used to collect reflection spectra using an internal polychromatic illuminant (fiber-optical reflection spectroscopy mode). In our configuration, this illuminant was switched off and the external UV source described previously was used instead.

To minimize the contribution of any reflection from the light source in the sensor detection range, we filtered the UV source using a lowpass filter (cutoff ~415 nm; Balcar). This removed the secondary emission peak at 425 nm. The resulting spectral irradiance was thus centered on 390 nm with a FWHM of approximately 40 nm. In addition, a longpass filter (2E, cut-on ~430 nm; Kodak Wratten) was placed in front of the acquisition fiber to filter out the reflection of the second order of emission from the source, centered at 780 nm, by the material and to minimize the distortion of the luminescence spectra. This filter combination, as well as the 45°/0° configuration of the excitation and emission paths, allowed an optimized collection of the luminescence light emitted by the object (Fig. 3). The corresponding spectra are presented Fig. 4.

The distance between the fiber optic spectrometer and the object was comparable among the successive pigment spectra acquisitions, but it varied when we gathered the illuminant spectra. Because we are interested only in the shape of the luminescence spectra, they have been plotted in arbitrary units, after subtraction of a dark spectrum. The acquisition time in this configuration was 34.82 s per spectrum.

DATA PROCESSING

An overview of the data processing we performed is outlined in Fig. 5. We first completed a series of preliminary corrections, which include noise reduction (dark-frame subtraction and flat-fielding) and band registration. We then proceeded with the spectral estimation, in our case based on a neural network using the spot luminescence spectra. Except when otherwise noted, all processing was performed using Matlab (7.12 R2011a).

Preliminary Corrections. ***Offset, Thermal, and Flat-Field Calibrations.*** To obtain a calibrated multispectral acquisition, in addition to the multispectral acquisitions of the scene, we acquired a set of dark frames and a set of images of the illumination heterogeneity. These shots were used for the dark-frame subtraction and flat-fielding. For every multispectral band, we performed an acquisition with the cap on the lens and the same acquisition time, a dark frame or thermal image. By subtracting the dark frame from the acquisition frame for each band, we corrected the systematic offset and thermal noise per pixel. To correct each image for the spatial heterogeneity of the illumination, we produced a master flat-field frame by averaging a set of frames representing a white scene in the same illumination and acquisition conditions as the acquisition frames. In practice, we imaged a sheet of paper in varying positions

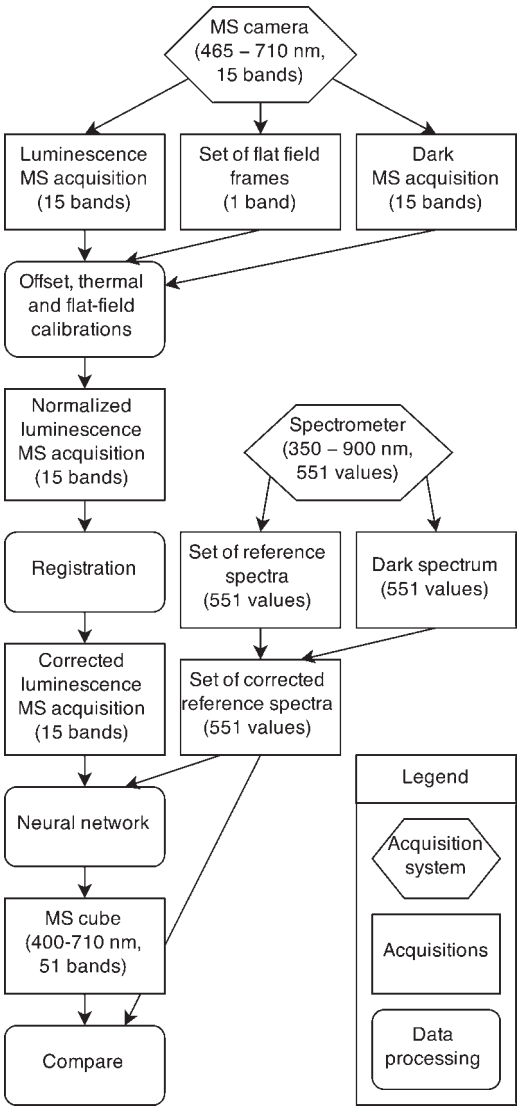

FIG. 5. Data processing overview.

at a given band. By averaging these acquisitions, we removed the contribution of the uneven background, for example dust on the paper itself. It was also possible to compute the median frame from the flat-field frames; this is less influenced by extreme values but requires a greater number of initial flat-field frames. The flat-field frames were also dark-frame subtracted to eliminate systematic offsets and thermal noise.

The corrected image of channel i, $\mathbf{U}_i$, was calculated from the raw image of channel i, $\mathbf{R}_i$, using:

$$\mathbf{U}_i = \frac{\mathbf{R}_i - \mathbf{T}_i}{\langle \mathbf{F}_J \rangle - \mathbf{T}_J^F} \times C \qquad (1)$$

where $\mathbf{T}_i$ is the thermal image related to channel i, $\langle \mathbf{F}_J \rangle$ is the average of the flat-field images (all flat-field images were taken for a given channel J), $\mathbf{T}_J^F$ is the thermal image related to the flat-field image, and $C = \langle \langle \mathbf{F}_J \rangle - \mathbf{T}_J^F \rangle$ is a multiplicative factor that keeps pixel values close to original because the flat-field images may be more saturated than the acquisitions. The division is a pixelwise division.

These noise reduction steps are commonly used in astronomical photography and multispectral imaging; similar approaches were described by Mansouri et al.[32] We thus corrected for the effects of vignetting (bright center and dark corners), blemishes on the lens and on the glass that protected the CCD, different pixels with different quantum efficiencies, and eventual illumination non-uniformity.

However, we did not correct for temporal noise, such as shot noise, nor did we take into account the effect of the blemishes on the filters. This last correction would have required several flat-field acquisitions per channel, tripling the total acquisition time if we were to use four flat-field frames per channel. It is also possible to acquire several images per wavelength and to average them to minimize the shot noise; this also greatly increases the total acquisition time.

The only correction we performed on the luminescence spectra was the subtraction of a dark spectrum obtained with the shutter closed and equivalent integration time from the acquisition spectra.

Registration. The variations in filter thickness and possible errors in the parallelism of the filters with respect to the lens introduce a misregistration of the images in the various bands that compose a multispectral acquisition. The chromatic aberration of an interference filter-wheel multispectral camera was modeled by Brauers et al.[29] They concluded that an affine transform is sufficient to compensate for the misregistration and spatially align the images obtained in the various channels.

In practice we corrected the misalignment using a simple translation, which gives satisfying results, using the StackReg[33] plug-in for ImageJ.[34]

Luminescence Estimation. ***Problem Statement.*** One interest of researchers using multispectral imaging is the possibility of retrieving, for each pixel of the scene, a spectrum that is comparable to reference data classically obtained using spot spectroscopy. However, this is not the case for the multispectral data treated with the preliminary corrections discussed in this article. In fact, these data do not account for the transmittance of the filters or for the sensitivity of the camera over the spectral range of interest; they still do not represent a multispectral luminescence cube. An additional step is necessary to obtain such data. This step is called luminescence estimation (or luminescence reconstruction) in reference to reflectance estimation[35] (or reflectance reconstruction[36]).

An illustration of the complex nature of the data obtained after the preliminary corrections can be found in the issue of data representation. At this stage, for each pixel the set of values can be plotted as the intensity versus, for instance, the center (maximal transmittance) wavelength of each filter.[19] This type of representation, however, is possibly incomplete and generates uncertainty in the final spectrum extracted because a set of bandpass filters generally has different characteristics (width, maximal transmittance, and shape of the transmittance curves) and partially overlapping transmittances. An attempt to represent the broadband nature of this discrete data is presented in Fig. 6.

The number and width of the bands necessary to obtain multispectral data comparable to the spectroscopic data

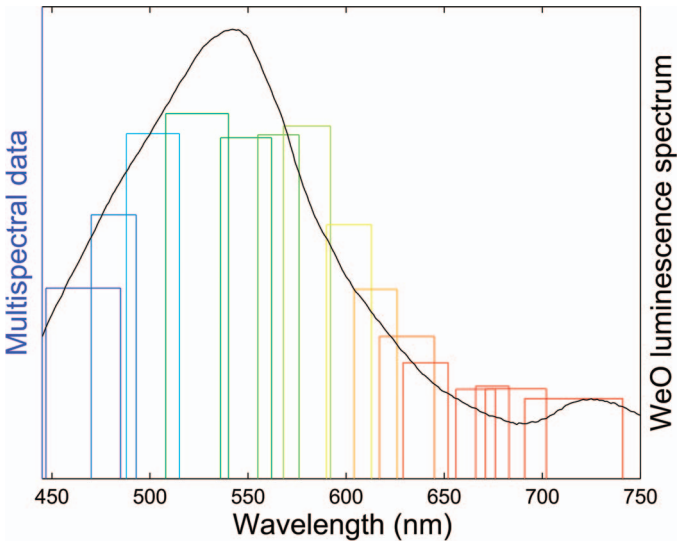

FIG. 6. Weld pigment in oil binder. The luminescence spectrum (solid black line) is compared to the multispectral acquisitions (colored histogram bars) for the same spot. The luminescence spectrum was collected on a few square millimeters and has a spectral resolution of 1 nm. The height of the histogram bars represents the pixel intensity, and their width represents the passband of the filters. The spectral data extracted from the multispectral data are averaged over an area of 5×5 pixels. Although this figure highlights the broadband nature of the data, it does not represent the varying exposure time between each filter. This exposure time is optimized per filter to cover the dynamics of the sensor over the full scene.

are crucial parameters, although no consensus exists in the literature. It is generally believed that the highest number of narrow bands provides optimal spectral data. However, this poses many practical problems, especially for luminescence imaging. Increasing the number of bands too much can annihilate the advantages of multispectral imaging compared to raster spot techniques due to the increase of the total acquisition time. The solution of increasing the flux of the source to increase the number of luminescent photons detected in each band can generate irradiation damage. This is thus strictly forbidden when light-sensitive materials are studied. In particular, increasing the number of bands implies increasing the acquisition time to obtain data with a comparable signal-to-noise ratio. The acquisition parameters are also dependent on the intrinsic luminescence properties of the materials under study, such as the sharpness and the complexity of the luminescence features. Previous luminescence studies reported the use of five to seven bands covering a range of 200–300 nm. This corresponds to a step of approximately 50 nm with 40 nm FWHM filters.[8,19,22] There are large discrepancies in the adequate number of bands recommended by different studies on multispectral reflection imaging (between 3 and 17).[37]

Theory. Luminescence estimation from a luminescence multispectral acquisition differs only slightly from reflection estimation from reflection multispectral acquisitions.[27] Because luminescence estimation has, to our knowledge, never been investigated in depth, we detail here the theory behind this method, simply extending models used for reflection estimation. Given the similarity of the methods and the dearth of literature on luminescence estimation, references and methods for both luminescence and reflection estimation are given throughout this section.

The recorded signal of the kth channel d_k (where $k \in [\![1, K]\!]$; in our case, $K = 15$) is a function of the luminescence $I(\lambda)$ of the surface, but also the transmittance of the kth filter $t_k(\lambda)$, the spectral sensitivity of the lens $o(\lambda)$, and the sensitivity of the CCD $c(\lambda)$. We assume the illuminant is completely filtered out, that is, that the recorded signal does not present any contribution of the reflection or stray light. We also assume noise has been removed by the preliminary corrections described previously. We assume a linear optoelectronic transfer function. Our goal is to solely recover $I(\lambda)$.

For a given pixel, the recorded signal of the kth channel is thus:

$$d_k = \int_{\lambda_{min}}^{\lambda_{max}} I(\lambda) t_k(\lambda) o(\lambda) c(\lambda) d\lambda \tag{2}$$

We replace $t_k(\lambda)o(\lambda)c(\lambda)$ by $S(\lambda)$, the spectral sensitivity of the kth channel. Equation 2 then becomes:

$$d_k = \int_{\lambda_{min}}^{\lambda_{max}} S(\lambda) I(\lambda) d\lambda \tag{3}$$

Regularly sampling the spectral range at N wavelengths, Eq. 3 becomes, in matrix notation:

$$d_k = \mathbf{S}_k^T(\lambda)\mathbf{I}(\lambda) \tag{4}$$

where $\mathbf{S}_k^T(\lambda) = [s_k(\lambda_1)\, s_k(\lambda_2) \ldots s_k(\lambda_N)]$ is the vector that describes the spectral sensitivity of the kth channel of the acquisition system, $\mathbf{I}(\lambda) = [I(\lambda_1)\, I(\lambda_2) \ldots I(\lambda_N)]^T$ is the vector of the sampled spectral response of the scene, and superscript T is the transpose operator. If we consider a system with all K channels, Eq. 4 can be written as:

$$\mathbf{d} = \mathbf{S}^T\mathbf{I} \tag{5}$$

where $\mathbf{d}$ is a vector containing all K camera outputs and $\mathbf{S} = [S_1\ S_2 \ldots S_K]$ is the matrix containing all the channels' spectral sensitivities $\mathbf{S\_k}$.

Our goal is to obtain $\mathbf{I}$, the luminescence of the scene for each pixel, given $\mathbf{d}$, the camera outputs. We thus need to calculate the operator $\mathbf{Q}$ that satisfies $\tilde{\mathbf{I}} = \mathbf{Qd}$, where $\tilde{\mathbf{I}}$ is the estimated luminescence. The variety of methods that can be used can be grouped in three categories based on how matrix $\mathbf{Q}$ is calculated, although some methods[38] are based on a combination of the following techniques.

Direct Physical System Characterization. It is possible to recover radiometrically calibrated data by correcting raw data from the detection chain of the system using the known filter transmittance and theoretical camera sensitivity. This is widely used both for reflection estimation[39–42] and luminescence estimation.[9] However, this method is based on a matrix inversion (or pseudo-

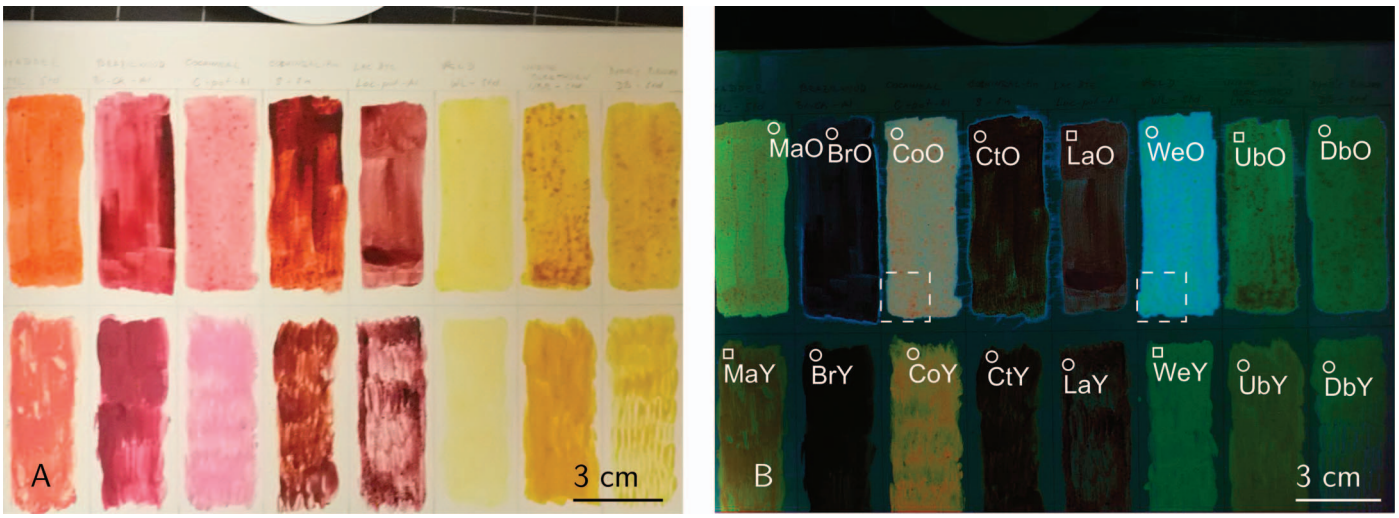

FIG. 7. Lake pigments panel. The pigments are in the order given in Table I. First row: linseed oil binder. Second row: egg yolk binder. (**A**) Under white light. (**B**) False color image composed of three images extracted from the multispectral acquisitions after noise reduction showing the position of the reference spectra. Blue channel: first multispectral band (centered at 465 nm, FWHM 30 nm). Green channel: central multispectral band (centered at 600 nm, FWHM 20 nm). Red channel: last multispectral band (centered at 710 nm, FWHM 40 nm). Circles represent the position of the spot spectra used to train the neural network while squares represent the position of the spot spectra used to evaluate the quality of the estimation. Symbols are larger than the actual sampling size to improve readability. The dashed boxes indicate the zones imaged in Fig. 9.

inverse), which makes it very vulnerable to noise and approximations.

Direct Interpolation of the Camera Outputs. This method has been explored for reflection estimation using polynomials.[43,44] Although it has been widely explored for reference patches, it is rarely used in practice. This is probably due to constraints related to the number of input and estimated channels, as well as the difficulty of choosing the best-order polynomial on unknown data.

Matching Areas of Known Spectral Response. Equation 5 can also be solved by indirectly matching a set of M patches of known luminescence with the corresponding multispectral outputs. Assuming M pairs of ($\mathbf{d}_m$, $\mathbf{I}_m$) from Eq. 5, we build a $K \times M$ matrix $\mathbf{D}$ and an $N \times M$ matrix $\mathbf{R}$. $\mathbf{Q}$ is obtained from

$$\mathbf{R} = \mathbf{QD} \tag{6}$$

through the pseudo-inverse of $\mathbf{D}$: $\mathbf{Q} = \mathbf{RD}^{+}$ (in which the superscript $+$ is the pseudo-inverse operator).

This matrix $\mathbf{Q}$ is then used to estimate the luminescence of all pixels of the multispectral acquisitions from the camera outputs. Equation 6 can be solved using any optimization method—for example, in the case of reflection estimation, least squares regression[25] or neural network.[26] It is also possible to use $N = K$ and $M = 1$ to easily calibrate luminescence data.[8] The choice of the single pair of matching spectra is a crucial parameter in this case.

The luminescence estimation used in this article is based on this third paradigm, matching a set of patches of known spectra using a neural network previously developed for reflection estimation.[45]

TABLE I. Paint films present on the painted panel and abbreviations used.

	Binder	
Lake pigment	Oil	Yolk
Al-madder	MaO	MaY
Al-brazilwood on chalk	BrO	BrY
Al-cochineal	CoO	CoY
Sn-cochineal	CtO	CtY
Al-lac dye	LaO	LaY
Al-weld	WeO	WeY
Unripe buckthorn	UbO	UbY
Dyer's broom	DbO	DbY

CASE STUDY

Lake Pigment Paints. We tested the selected method on a panel composed of 16 model paint patches prepared in March 2011 during a workshop on the making of historical lake pigments (Back to the Roots CHARISMA workshop, Dörner Institut). The 16 patches consisted of eight lake pigments mixed in two different binders: linseed oil (top row) or egg yolk (bottom row). The lake pigments were prepared according to historical recipes. Lake pigments are a family of historical pigments in which the organic molecules extracted from vegetal (madder, dyer's broom, buckthorn, weld, and brazilwood) or animal (cochineal, kermes, and lac dye) dyestuffs are mordanted with inorganic substances.[28,46,47] The panel is shown under white light in Fig. 7A, and the list of pigments and their abbreviation is given in Table I.

The patches exhibit a strong diversity in terms of luminescence spectral emission and yields. Emission spectra were collected for all 16 patches using the ASD FieldSpec 4 spectroradiometer, described previously, over a few square millimeters at the spatial locations shown in Fig. 7B. These spectra are shown in Fig. 8.

The interpretation of the spectral features observed in the emission spectrum of each patch is not extensively discussed here because it is outside the scope of this article. However, despite the contribution of the excitation source in the visible, these spectra correspond to the literature. Briefly, the local maxima for the red paints

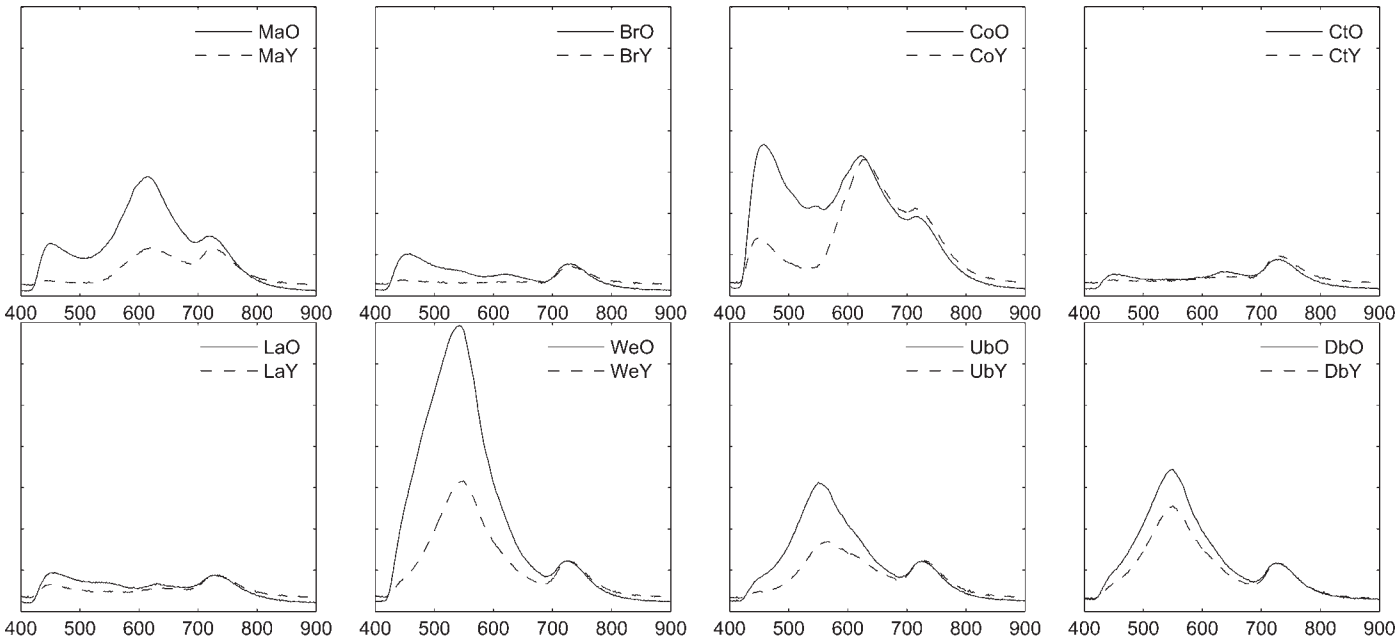

FIG. 8. Luminescence emission spectra of the lake pigment paint films given as a function of the wavelength (in nanometers). Solid line: oil binder. Dashed line: egg yolk binder. Excitation, 370–410 nm. Intensity given in arbitrary units. The acquisition time for all spectra is 34.82 s.

in the 600–640 nm region can be assigned to the previously reported luminescence of red lake pigments.[6,13,21] Similarly, the local maxima for the yellow paints in the 540–560 nm region can be assigned to the luminescence of yellow lake pigments, even though literature on this matter is scarcer.[48] Also, the luminescence of the binder[49] and complex optical (auto-) absorption effects[6,50] contribute to alter the luminescence of the lake pigments. The local peak around 730 nm, visible for all the pigments, is most probably due to the reflection of the stray light from the source, which can be observed in Fig. 4.

Of the 16 reference spectra, we used 12 as a training set for the neural network and used the remaining four to evaluate the accuracy of the spectral estimation. These evaluation spectra correspond to four different lake pigments, two in an oil binder and two in an egg binder; two red pigments and two yellow pigments. This partition between training and evaluation spectra thus represents a sensible choice of spectra as a training set.

For each patch, the multispectral data were averaged over an area of 5×5 pixels, which corresponds to an area of approximately 1 mm^2. We chose this size and the position to best match the integration area and the position of the reference spectra collected on the panel; however, it was difficult to know the exact position and area over which the spot spectra were collected. The luminescence spectra are reconstructed with a 5 nm step between 460 and 710 nm. Fig. 7B shows the position of both the reference positions used as a training set and those used to evaluate the reconstruction accuracy.

Results. The result of the spectral reconstruction is a multispectral cube, that is, a data cube composed of two spatial dimensions and one spectral dimension. Two representations of such a cube are given in Fig. 9 and compared to the data prior to processing. Figure 9 illustrates that, for each pixel of the image, an improved spectrally resolved spectrum is obtained while preserving the spatial resolution inherent in the imaging system.

The measured and reconstructed spectra show strong similarities based on a simple qualitative observation. Figure 10 shows the training spectra used for the neural network and the corresponding reconstructed spectra, and Fig. 11 shows the acquired luminescence spectra and the corresponding reconstructed spectra used to evaluate the neural network. The discrepancies revealed by a visual comparison of the measured and reconstructed spectra are mostly small differences in intensity and dynamics for wavelengths longer than 690 nm. This is probably due to the larger spectral width of the last bandpass filter used in the multispectral acquisition (Figs. 2 and 6), combined with the contribution of the reflection due to stray visible light around 730 nm.

The general shape and position of the local maxima are identical. Only two patches, UbY and MaO (both part of the training set), exhibit a non-visually satisfying accordance. In the case of UbY, this difference produces a slight shift in local peak maximum: 570 nm for the reconstructed spectrum instead of 565 nm for the measured spectrum. The patch MaO is satisfyingly reconstructed, except for the 460–560 nm range, in which the local minimum is less pronounced than in the measured spectrum.

We calculate the goodness-of-fit coefficient (GFC) between the reconstructed spectra and the luminescence spectra for the reference data and the remaining four spectra. The GFC is a metric proposed by Hernández-Andrés et al.[51] to compare a measured spectrum s_m to a reconstructed spectrum s_r. It is based on the Schwartz inequality and is defined as:

$$\mathrm{GFC} = \frac{\left|\sum_j s_m(\lambda_j) s_r(\lambda_j)\right|}{\sqrt{\sum_j s_m(\lambda_j)^2}\sqrt{\sum_j s_r(\lambda_j)^2}} \qquad (7)$$

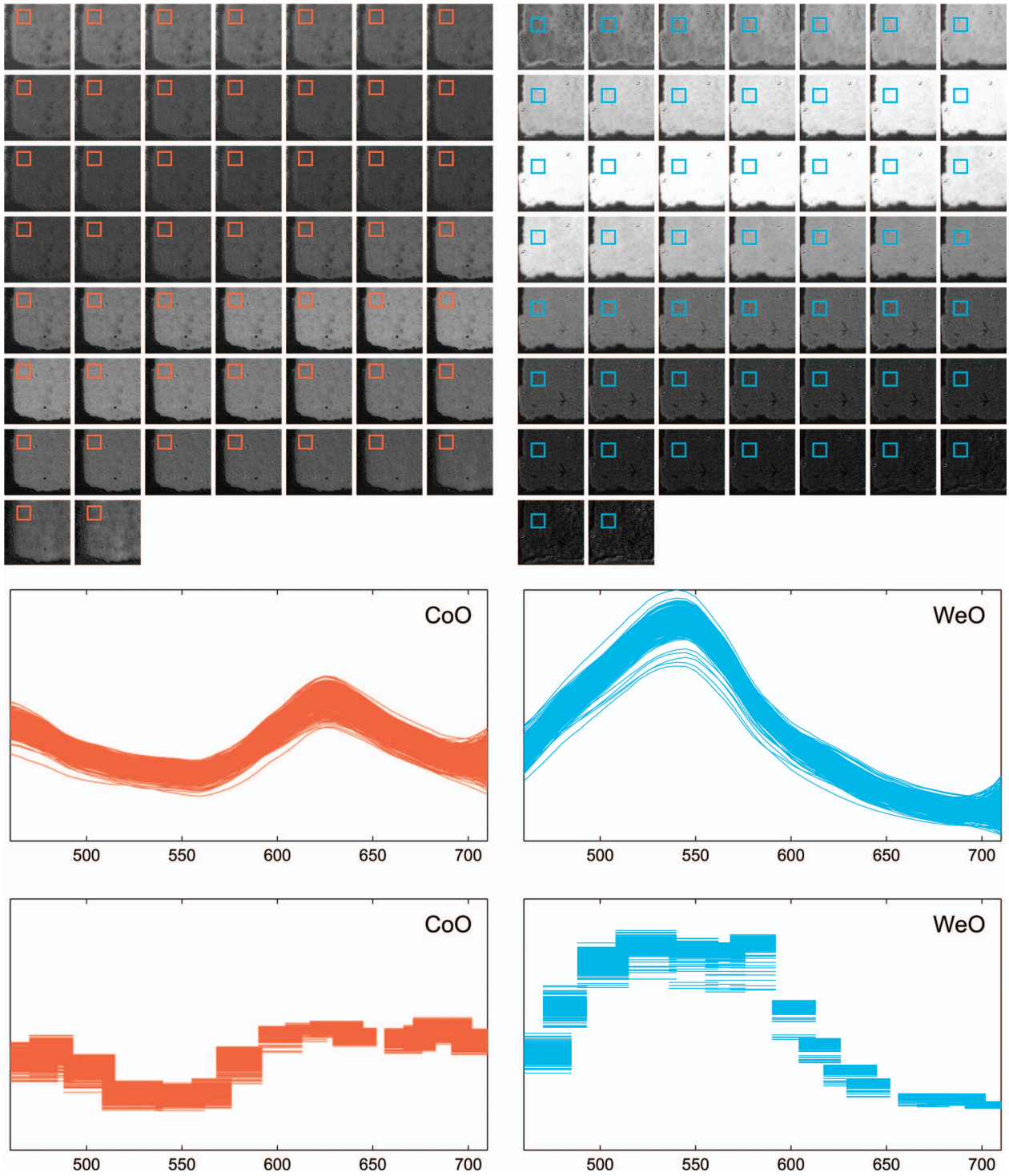

FIG. 9. Results of the neural network processing for two zones from Fig. 7B, corresponding to CoO (left) and WeO (right) patches. (**top**) Representation of the multispectral cube as a series of 51 grayscale images for these zones (one image per band, between 460 and 710 nm with a 5 nm step). Each colored box represents an area of 20 × 20 pixels. (**center**) Representation of the same multispectral cube as a series of 400 spectra corresponding to the 20 × 20 pixel box. (**bottom**) Representation of the 15-band multispectral acquisition (prior to neural network processing) corresponding to the 20 × 20 pixel box.

The GFC is a value between 0 and 1, where 1 corresponds to an exact match. Hernández-Andrés et al. defined an accurate match as one for which GFC > 0.995 and defined a good match as one for which GFC > 0.999. This metric is scale invariant, which is not the case for other widely used metrics such as root mean square error (RMSE). As such, the GFC is adequate to compare the shape of two spectra and is often used to evaluate the accuracy of spectral reconstructions.[35,45,52,53]

The GFCs between our reconstructed spectra and the luminescence spectra were calculated for the reference data used to train the neural network and for the remaining four positions used to evaluate the accuracy

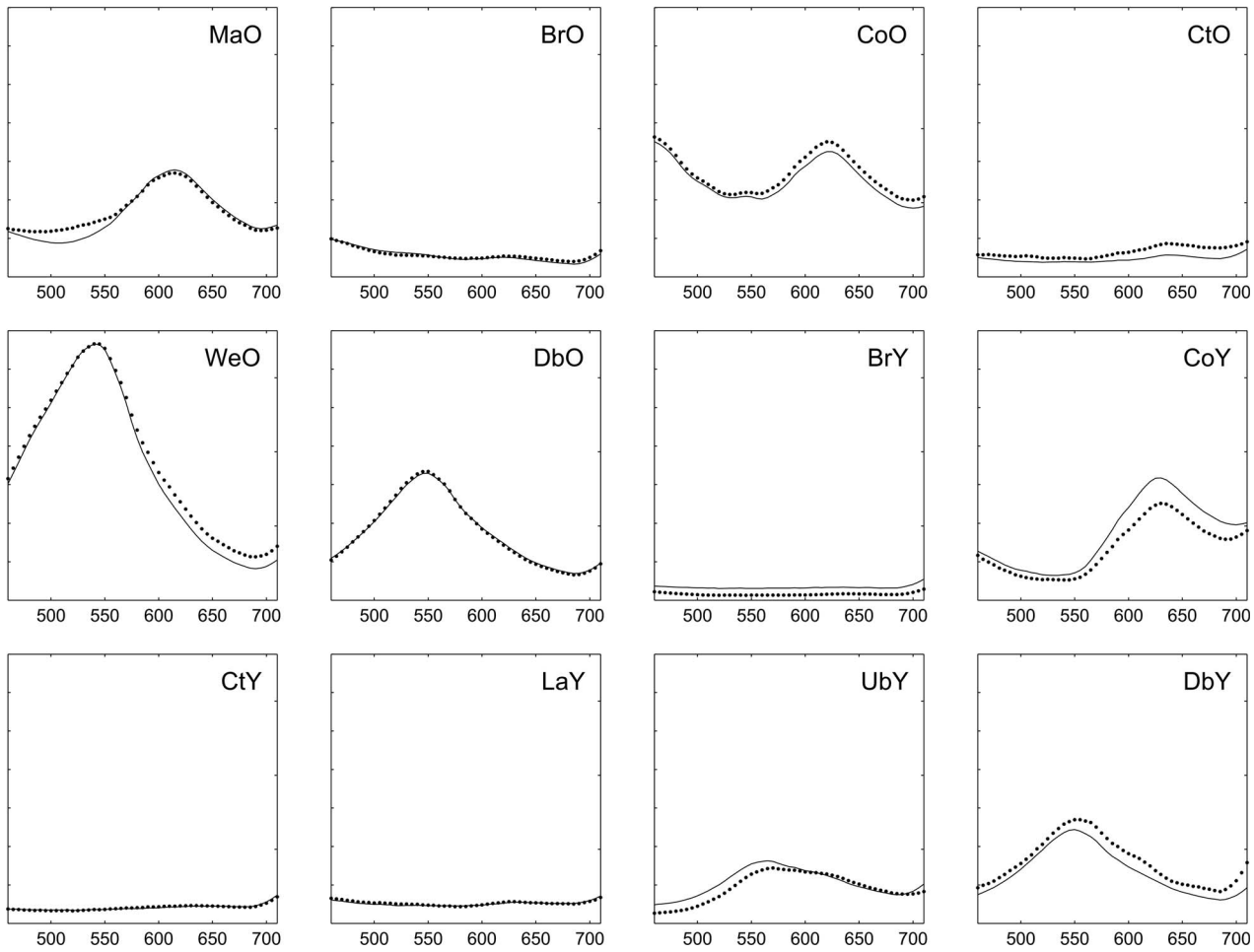

FIG. 10. Luminescence spectra (solid line) of the paint films used as the training set for the neural network and the corresponding reconstructed spectra (points). The spectra are reconstructed between 460 and 710 nm with a 5 nm step.

of the reconstruction (Table II). The quality of the reconstruction performed over a slightly reduced spectral range (from 460 to 690 nm) was also evaluated. We expected that the luminescence reconstruction would be improved if we reduced the reconstruction to a range with a reduced contribution of reflection.

For both reconstruction ranges, the spectral reconstruction is at least accurate (i.e., $1 - \mathrm{GFC} < 0.005$), if not good (i.e., $1 - \mathrm{GFC} < 0.001$), for most pigments. However, for three paint films (MaY, UbY, and UbO) the reconstruction cannot be defined as accurate. In the case of UbY, this simply confirms the visual observation. The reconstruction of the spectra for UbO is not accurate as defined by Hernández-Andrés et al.; however, it is close when the reconstruction is performed on the reduced range. As for MaO, the reconstruction is accurate despite the differences observed around 500 nm.

The reduction of the reconstruction range globally increases the quality of the reconstruction (a slight improvement of 0.0003 on the average GFC). In particular, the GFC of LaO is greatly improved (an accurate reconstruction becomes a good reconstruction). However, five spectra are negatively affected when we use the

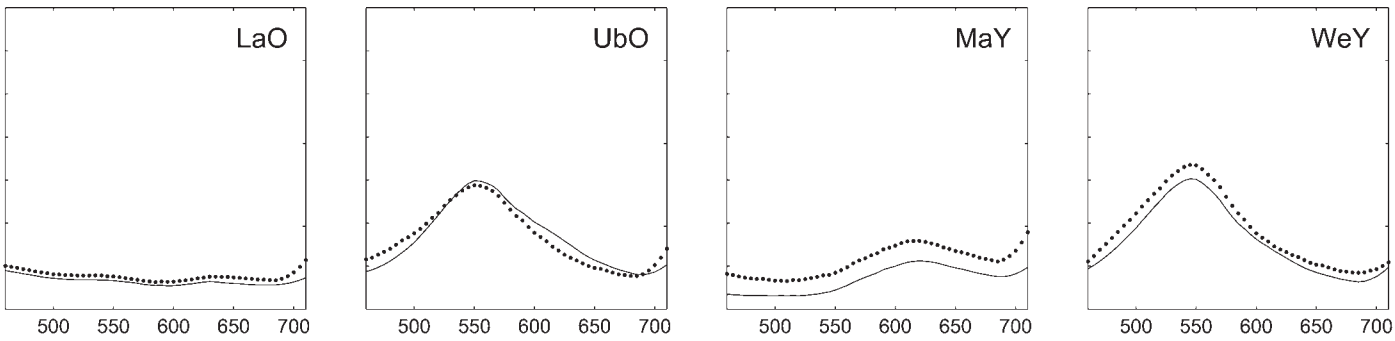

FIG. 11. Luminescence spectra (solid line) and the corresponding reconstructed spectra (points) of the paint films used to evaluate the neural network. The spectra are reconstructed between 460 and 710 nm with a 5 nm step.

TABLE II. Quality of two reconstruction ranges with a 5 nm step.[a]

	Reconstruction range (nm)	
Pigment	460–710	460–690
Training spectra		
MaO	0.0048	0.0049
BrO	0.0032	0.0027
CoO	0.0003	0.0002
CtO	0.0041	0.0044
WeO	0.0013	0.0011
DbO	0.0002	0.0002
BrY	0.0048	0.0050
CoY	0.0008	0.0006
CtY	0.0009	0.0007
LaY	0.0010	0.0008
UbY	0.0106	0.0110
DbY	0.0034	0.0018
Evaluation spectra		
LaO	0.0025	0.0004
UbO	0.0059	0.0052
MaY	0.0095	0.0098
WeY	0.0007	0.0007
Average	0.0034	0.0031

[a] Quality is given as $1 - \mathrm{GFC}$ to ease data interpretation and comparison. An accurate fit is one for which $1 - \mathrm{GFC} < 0.005$.

reduced reconstruction range, the ones for MaO, CtO, BrY, UbY, and MaY. Of these, UbY and MaY, as noted previously, are not accurately reconstructed. The fact that the reduction of the reconstruction range, which globally improves the reconstruction, has a negative effect on these two positions suggests that we cannot accurately reconstruct these two spectra using our data. For MaO, CtO, and BrY, the reduction in GFC introduced by the reduction of the reconstruction range is small (between 0.0001 and 0.0003). In addition, CtO and BrY present quasi-flat spectra, exhibiting low luminescence in the current conditions.

DISCUSSION

Until now, the interpretation of in situ luminescence data of historical paints has been based mostly on the detection of emission peaks and local maxima at given wavelengths (presence or absence).[4,6,11] In some cases, the shapes of the peaks and their relative intensities have also been studied.[9] However, the identification of materials based on their luminescence properties has been hampered by the optical distortion of the photoluminescence properties of individual materials when admixed. This is due, for example, to complex reabsorption and secondary luminescence effects, which depend on the optical properties of these materials.[4,50] The method presented here quite efficiently retrieves the shapes of the spectra as shown by the GFC metric and qualitative visual observation. It thus seems to offer promising improvements for the field of in situ luminescence.

The accuracy of a reconstruction is strongly dependent on the adequacy between the training data and the scene being analyzed. The training spectra must be representative of the surface of interest. By representative, we mean that this set of spectra must cover the same dynamics in intensity and must present emissions with spectral widths that are close to those of the materials of the scene being analyzed. The training spectra do not necessarily have to be spectra of the same materials as those of the scene, but they must be spectra of materials with comparable properties (e.g., the range of emission and the variation of quantum yields). The easiest way to check the efficiency of a spectral estimation is to compare it with spot analysis from the scene. In practice, at least in the case of reflection estimation, this step is not often systematically performed.

An external calibration target using known spectra is often used to provide the training spectra in the case of reflection estimation. In particular, the ColorChecker Classic (24 patches), ColorChecker Digital SG (140 patches), and ColorChecker DC (237 patches) are common choices in this case.[26] Occasionally, these matte reflection standards are coated with a varnish to create a glossy reflection standard that matches the reflection properties of the object under study (paintings, for example).[25] The appropriate number of training spectra depends on the multispectral acquisition system and on the object under study.

Another approach consists of composing a training set by acquiring a set of spot spectra from the object of interest using a spectrophotometer. However, relying on selected points on objects means we cannot reconstruct unidentified areas. This is not a problem when we are studying objects in which the various areas are sharply delimited, such as reference panels or paintings made of juxtaposed areas of monochrome paints (homogeneous at the scale of observation).[19] However, when we are studying the spectral variety of an area, it is difficult to anticipate the number and position of areas that are necessary for a pertinent training of the neural network. In such cases, the potentials of multispectral imaging are more general because it can be used to study the spectral variety of an area.

CONCLUSION AND PERSPECTIVES

We have shown that a neural network can be adapted to reconstruct luminescence spectra from noise-corrected multispectral acquisitions. The neural network not only provides us with an estimation of the luminescence spectra for each pixel, it also simultaneously corrects the noise introduced by the instrumentation without our having to characterize each element independently. The retrieval of spectral information of improved spectral resolution is fundamental for material characterization. This is a promising technique, although many parameters (choice and number of training spectra) must still be investigated in depth.

The resulting multispectral cubes can be processed per band using regular image-processing techniques (e.g., to improve readability and contrast) or per pixel using signal-processing techniques (e.g., finding maxima, deconvolution, and spectral angle mapping [SAM]). The current challenge is to develop algorithms to process the full cube using integrated approaches across all three dimensions, for example, a SAM that takes into account spatial proximity.

Luminescence multispectral imaging is largely based on the development performed in reflection configuration. Even though reflection imaging is a more mature field,

many fundamental questions have still not been clearly answered. For example, there is no consensus on the number of necessary acquisition bands. Although many systems acquire 31 bands between 400 and 700 nm (i.e., one channel every 10 nm), Berns et al.[54] stated that comparable spectral precision can be obtained using fewer than 10 bands. There is also no consensus on how to create an optimal reference target (how many patches, their characteristics, etc.) because the adequacy of such targets is both acquisition system and object dependent.

The same fundamental problems are present in luminescence multispectral imaging, with additional difficulties. In particular, luminescence imaging is illuminant dependent, whereas reflection imaging is illuminant independent. There is also generally a high variation in the luminescence intensity, depending on the materials studied. However, the luminescence properties of cultural heritage surfaces generally present low intensities. The long acquisition times necessary under these conditions introduce a high level of noise.

Future work should include the optimization of the light source to minimize its emission in the spectral imaging range and the creation of a reference chart for luminescence multispectral imaging. The challenge of this last task is mostly due to the great variability in the intensity of the materials and the required acquisition times. To be used to train a neural network, the reference chart must be acquired under the same conditions as the surface of interest (same illuminant, same acquisition time per channel, etc.). The luminescence of the materials that compose such a luminescence reference chart must be adapted to the setup dynamics and the acquisition time. This reference chart will be used to reconstruct spectra for our future study of historical violin varnishes.

ACKNOWLEDGMENTS

This research is conducted in the framework a PNRCC program for conservation science, supported by the Department for Research, Higher Education and Technology of the French Ministère de la Culture. Stéphane Vaiedelich (Laboratoire de recherche et de restauration, Musée de la musique), and Christine Andraud and Bertrand Lavédrine (Centre de Recherche sur la Conservation des Collections) are gratefully acknowledged for their essential support in the project; Sophie Darribère (Musée de la musique) for the first development of the data processing; Alessandra Vichi (Institut photonique d'analyse non-destructive européen des matériaux anciens) for measuring the transmittance of the filters plotted in Fig. 2; and Alamin Mansouri (Le2i, Université de Bourgogne) for providing the neural network algorithm and Matlab code. The lake paints panel was created during a CHARISMA workshop (http://www.doernerinstitut.de/en/projekte/charisma/charisma_3.html). The CHARISMA project is co-funded by the European Commission under the action "Research Infrastructures" of the Capacities Programme GA No. FP7- 228330 (http://www.charismaproject.eu/).

1. J.J. Rorimer. Ultra-Violet Rays and Their Use in the Examination of Works of Art. New York: Metropolitan Museum of Art, 1931.
2. S.F. Sacconi. I Segreti di Stradivari. Cremona, Italy: Libreria del Convegno, 1972.
3. B. Brandmair, S.-P. Greiner, J. Röhrmann. Stradivari Varnish: Scientific Analysis of His Finishing Technique on Selected Instruments. Vienna: Serving Audio, 2010.
4. E.R. de la Rie. "Fluorescence of Paint and Varnish Layers. (Parts I-III)". Stud. Conserv. 1982. 27(1): 1-7; 27(2): 65-69; 27(3): 102-108.
5. T. Miyoshi. "Fluorescence from Pigments in Fresh and Stored Oil Colours Under N_2 Laser Excitation". Jpn. J. Appl. Phys. 1985. 24(8): 1113-1114.
6. C. Clementi, B. Doherty, P. Gentili, C. Miliani, A. Romani, B. Brunetti, A. Sgamellotti. "Vibrational and Electronic Properties of Painting Lakes". Appl. Phys. A.: Mater. Sci. Process. 2008. 92(1): 25-33. doi:10.1007/s00339-008-4474-6.
7. A. Nevin, J.-P. Echard, M. Thoury, D. Comelli, G. Valentini, R. Cubeddu. "Excitation Emission and Time-Resolved Fluorescence Spectroscopy of Selected Varnishes Used in Historical Musical Instruments". Talanta. 2009. 80(1): 286-293.
8. M. Thoury, J.K. Delaney, E.R. de la Rie, M. Palmer, K. Morales, J. Krueger. "Near-Infrared Luminescence of Cadmium Pigments: In Situ Identification and Mapping in Paintings". Appl. Spectrosc. 2011. 65(8): 939-951.
9. L. Bertrand, M. Réfrégiers, B. Berrie, J.-P. Echard, M. Thoury. "A Multiscalar Photoluminescence Approach to Discriminate Among Semiconducting Historical Zinc White Pigments". Analyst. 2013. 138(16): 4463-4469.
10. M. Elias, C. Magnain, C. Barthou, A. Nevin, D. Comelli, G. Valentini. "UV–Fluorescence Spectroscopy for Identification of Varnishes in Works of Art: Influence of the Under Layer on the Emission Spectrum". In: L. Pezzati, R. Salimbeni, editors. O3A: Optics for Arts, Architecture, and Archaeology II. Proc. SPIE. 2009. 7391: 739104. doi:10.1117/12.825093.
11. C. Clementi, C. Miliani, A. Romani, G. Favaro. "In Situ Fluorimetry: A Powerful Non-Invasive Diagnostic Technique for Natural Dyes Used in Artefacts: Part I. Spectral Characterization of Orcein in Solution, on Silk and Wool Laboratory-Standards and a Fragment of Renaissance Tapestry". Spectrochim. Acta, Part A. 2006. 64(4): 906-912.
12. G. Bottiroli, A.G. Galassi, E. Bernacchi. "Microspectrofluorometric Techniques as Applied to the Analysis of Binding Media and Varnishes in Color Samples Taken from Paintings". In: P.L. Parrini, editor. Scientific Methodologies Applied to Works of Art. Symposium presented at: Florence, Italy; May 2–5, 1984. Milan: Montedison progetto cultura, 1986. Pp. 168-170, 241.
13. A. Claro, M.J. Melo, S. Schäfer, J.S.S. de Melo, F. Pina, K.J. van den Berg, A. Burnstock. "The Use of Microspectrofluorimetry for the Characterization of Lake Pigments". Talanta. 2008. 74(4): 922-929.
14. L. Bertrand, M. Thoury, E. Anheim. "Ancient Materials Specificities for Their Synchrotron Examination and Insights into Their Epistemological Implications". J. Cult. Herit. 2013. 14(4): 277-289.
15. A. Casini, F. Lotti, M. Picollo, L. Stefani, A. Aldrovandi. "Fourier Transform Interferometric Imaging Spectrometry: A New Tool for the Study of Reflectance and Fluorescence of Polychrome Surfaces". In: J.H. Townsend, K. Eremin, A. Adriaens, editors. Conservation Science 2002: Papers from the Conference Held in Edinburgh, Scotland, May 22–24, 2002. London: Archetype Publications, 2003. Pp. 249-253.
16. A. Pelagotti, L. Pezzati, A. Piva, A. Del Mastio. "Multispectral UV Fluorescence Analysis of Painted Surfaces". Paper presented at: EUSIPCO 2006, 14th European Signal Processing Conference., Firenze, Italy; September 4-8 2006.
17. A. Pelagotti, A. Del Mastio, A. De Rosa, A. Piva. "Multispectral Imaging of Paintings". IEEE Signal Proc. Mag. 2008. 25(4): 27-36.
18. D. Comelli, G. Valentini, A. Nevin, A. Farina, L. Toniolo, R. Cubeddu. "A Portable UV-Fluorescence Multispectral Imaging System for the Analysis of Painted Surfaces". Rev. Sci. Instrum. 2008. 79(8): 086112.
19. J.K. Delaney, J.G. Zeibel, M. Thoury, R. Littleton, M. Palmer, K.M. Morales, E.R. de la Rie, A. Hoenigswald. "Visible and Infrared Imaging Spectroscopy of Picasso's Harlequin Musician: Mapping and Identification of Artist Materials in Situ". Appl. Spectrosc. 2010. 64(6): 584-594.
20. D. Comelli, C. D'Andrea, G. Valentini, R. Cubeddu, C. Colombo, L. Toniolo. "Fluorescence Lifetime Imaging and Spectroscopy as Tools for Nondestructive Analysis of Works of Art". Appl. Opt. 2004. 43(10): 2175-2183.
21. A. Claro, M.J. Melo, J.S. Seixas de Melo, K.J. van den Berg, A. Burnstock, M. Montague, R. Newman. "Identification of Red Colorants in van Gogh Paintings and Ancient Andean Textiles by Microspectrofluorimetry". J. Cult. Herit. 2010. 11(1): 27-34.
22. M. Thoury, J.-P. Echard, M. Réfrégiers, B. Berrie, A. Nevin, F. Jamme, L. Bertrand. "Synchrotron UV-Visible Multispectral Luminescence Microimaging of Historical Samples". Anal. Chem. 2011. 83(5): 1737-1745.
23. R. Fantoni, L. Caneve, F. Colao, L. Fiorani, A. Palucci, R. Dell'Erba, V. Fassina. "Laser-Induced Fluorescence Study of Medieval Frescoes by Giusto de' Menabuoi". J. Cult. Herit. 2013. 14(3): S59-S65.

24. T. Hirvonen, N. Penttinen, M. Hauta-Kasari, M. Sorjonen, K.-E. Peiponen. ‘‘A Wide Spectral Range Reflectance and Luminescence Imaging System’’. Sensors. 2013. 13(11): 14500-14510.
25. K. Martinez, J.S. Cupitt, D. Saunders, R. Pillay. ‘‘Ten Years of Art Imaging Research’’. Proc. IEEE. 2002. 90(1): 28-41.
26. A. Ribés, F. Schmitt. ‘‘A Fully Automatic Method for the Reconstruction of Spectral Reflectance Curves by Using Mixture Density Networks’’. Pattern Recogn. Lett. 2003. 24(11): 1691-1701.
27. C. Simon Chane, A. Mansouri, F.S. Marzani, F. Boochs. ‘‘Integration of 3D and Multispectral Data for Cultural Heritage Applications: Survey and Perspectives’’. Image Vision Comput. 2013. 31(1): 91-102.
28. J. Kirby, M. van Bommel, A. Verhecken. Natural Colorants for Dyeing and Lake Pigments. London: Archetype Publications, 2014.
29. J. Brauers, N. Schulte, T. Aach. ‘‘Multispectral Filter-Wheel Cameras: Geometric Distortion Model and Compensation Algorithms’’. IEEE Trans. Image Process. 2008. 17(12): 2368-2380.
30. A. Mansouri, F.S. Marzani, J.Y. Hardeberg, P. Gouton. ‘‘Optical Calibration of a Multispectral Imaging System Based on Interference Filters’’. Opt. Eng. 2005. 44(2): 027004.
31. M. Yamaguchi, H. Haneishi, N. Ohyama. ‘‘Beyond Red-Green-Blue (RGB): Spectrum-Based Color Imaging Technology’’. J. Imaging Sci. Technol. 2008. 52(1): 01020-1.
32. A. Mansouri, F.S. Marzani, P. Gouton. ‘‘Development of a Protocol for CCD Calibration: Application to a Multispectral Imaging System’’. Int. J. Robot. Autom. 2005. 20(2): 94-100.
33. P. Thévenaz, U. Ruttimann, M. Unser. ‘‘A Pyramid Approach to Subpixel Registration Based on Intensity’’. IEEE Trans. Image Process. 1998. 7(1): 27-41.
34. W.S. Rasband. ‘‘ImageJ’’. U.S. National Institutes of Health. 2012. http://imagej.nih.gov/ij/.
35. F.H. Imai, L.A. Taplin, E.A. Day. Comparative Study of Spectral Reflectance Estimation Based on Broad-Band Imaging Systems. Technical Report. Rochester, NY: Rochester Institute of Technology, Carson Center for Imaging Science, Munsell Color Science Laboratory, 2003.
36. Y. Zhao, R.S. Berns. ‘‘Image-Based Spectral Reflectance Reconstruction Using the Matrix R Method’’. Color Res. Appl. 2007. 32(5): 343-351.
37. D. Connah, A. Alsam, J.Y. Hardeberg. ‘‘Multispectral Imaging: How Many Sensors Do We Need?’’. In: Twelfth Color Imaging Conference: Color Science and Engineering Systems, Technologies, and Applications. Springfield, VA: Society for Imaging Science and Technology, 2004. Pp. 53-58.
38. H.-L. Shen, H.-J. Wan, Z.-C. Zhang. ‘‘Estimating Reflectance from Multispectral Camera Responses Based on Partial Least-Squares Regression’’. J. Electron. Imaging. 2010. 19(2): 020501.
39. F.H. Imai, R.S. Berns. ‘‘Spectral Estimation Using Trichromatic Digital Cameras’’. In: Proceedings of the International Symposium on Multispectral Imaging and Color Reproduction for Digital Archives. Chiba, Japan: Chiba University, 1999. Pp. 42-49.
40. H.-L. Shen, P.-Q. Cai, S.-J. Shao, J.H. Xin. ‘‘Reflectance Reconstruction for Multispectral Imaging by Adaptive Wiener Estimation’’. Opt. Express. 2007. 15(23): 15545-15554.
41. S. Tominaga. ‘‘Multichannel Vision System for Estimating Surface and Illumination Functions’’. J. Opt. Soc. Am. A. 1996. 13(11): 2163-2173.
42. X. Zhang, H. Xu. ‘‘Reconstructing Spectral Reflectance by Dividing Spectral Space and Extending the Principal Components in Principal Component Analysis’’. J. Opt. Soc. Am. A. 2008. 25(2): 371-378.
43. S. Bianco, F. Gasparini, R. Schettini, L. Vanneschi. ‘‘Polynomial Modeling and Optimization for Colorimetric Characterization of Scanners’’. J. Electron. Imaging. 2008. 17(4): 043002.
44. D.R. Connah, J.Y. Hardeberg. ‘‘Spectral Recovery Using Polynomial Models’’. In: R. Eschbach, G.G. Marcu, editors. Color Imaging X: Processing, Hardcopy and Applications. Proc. SPIE. 2005. 5667: 65-75. doi:10.1117/12.586315.
45. M. Sanchez, A. Mansouri, F.S. Marzani, P. Gouton. ‘‘Spectral Reflectance Estimation from Multispectral Images Using Neural Networks’’. Paper presented at: Fourth International Conference on Physics in Signal and Image Processing (PSIP’2005). Toulouse, France; January 21–February 2, 2005.
46. J. Kirby, M. Spring, C. Higgitt. ‘‘The Technology of Red Lake Pigment Manufacture: Study of the Dyestuff Substrate’’. National Gallery Tech. Bull. 2005. 26(1): 71-87.
47. J. Kirby, M. Spring, C. Higgitt. ‘‘The Technology of Eighteenth- and Nineteenth-Century Red Lake Pigments’’. National Gallery Tech. Bull. 2007. 28(1): 69-96.
48. Y. Matsuda. ‘‘Non-Destructive Analysis of Yellow Natural Dyestuffs by Three-Dimensional Fluorescence Spectroscopy’’. Bunkazai Hozon-Syuhuku Gakkaisi. 1997. 41: 54-63.
49. A. Nevin, D. Comelli, G. Valentini, R. Cubeddu. ‘‘Total Synchronous Fluorescence Spectroscopy Combined with Multivariate Analysis: Method for the Classification of Selected Resins, Oils, and Protein-Based Media Used in Paintings’’. Anal. Chem. 2009. 81(5): 1784-1791.
50. G. Verri, C. Clementi, D. Comelli, S. Cather, F. Piquée. ‘‘Correction of Ultraviolet-Induced Fluorescence Spectra for the Examination of Polychromy’’. Appl. Spectrosc. 2008. 62(12): 1295-1302.
51. J. Hernández-Andrés, J. Romero, R.L. Lee. ‘‘Colorimetric and Spectroradiometric Characteristics of Narrow-Field-of-View Clear Skylight in Granada, Spain’’. J. Opt. Soc. Am. A. 2001. 18(2): 412-420.
52. F.H. Imai, L.A. Taplin, E.A. Day. ‘‘Comparison of the Accuracy of Various Transformations from Multi-Band Images to Reflectance Spectra’’. Technical Report. Rochester, NY: Rochester Institute of Technology, Carson Center for Imaging Science, Munsell Color Science Laboratory, 2002.
53. R. Jolivot, P. Vabres, F. Marzani. ‘‘Reconstruction of Hyperspectral Cutaneous Data from an Artificial Neural Network-Based Multispectral Imaging System’’. Comput. Med. Imag. Grap. 2011. 35(2): 85-8.
54. R.S. Berns, L. Taplin, M. Nezamabadi, M. Mohammadi, Y. Zhao. ‘‘Spectral Imaging Using a Commercial Color-Filter Array Digital Camera’’. In: I. Verger, editor. International Council of Museums Committee for Conservation: 14th Triennial Meeting, The Hague, The Netherlands, September 2005. Leeds, UK: Maney, 2005. Pp. 743-750.